Accepted Article Preview: Published ahead of advance online publication

Photonic Control of Thermal Radiation for Protective Windows

Yunbin Ying, Jianbo Yu, Weidong Shen, Pintu Ghosh, Min Qiu, and Qiang Li

Cite this article as: Yunbin Ying, Jianbo Yu, Weidong Shen, Pintu Ghosh, Min Qiu, and Qiang Li. Photonic Control of Thermal Radiation for Protective Windows. *Light: Advanced Manufacturing* accepted article preview 16 April, 2025; doi: 10.37188/lam.2025.034

Received 11 June 2024; revised 14 April 2025; accepted 15 April 2025; Accepted article preview online 16 April 2025

Photonic Control of Thermal Radiation for Protective Windows

Yunbin Ying[1], Jianbo Yu[1], Weidong Shen[1], Pintu Ghosh[1,], Min Qiu[2], and Qiang Li[1,*]*

[1]*State Key Laboratory of Extreme Photonics and Instrumentation, College of Optical Science and Engineering, Zhejiang University, Hangzhou 310027, China*

[2]*Key Laboratory of 3D Micro/Nano Fabrication and Characterization of Zhejiang Province, School of Engineering, Westlake University, Hangzhou 310024, China*

*qiangli@zju.edu.cn；*ghosh@zju.edu.cn

Abstract

Thermal protection and comfort are essential for instruments and humans, especially in high-temperature scenarios such as fires and steelworks. Existing thermal protective windows absorb external radiation and heat when exposed to thermal sources, thereby failing to provide thermal comfort to users. Herein, we present a nanophotonic-engineered thermal protective window (NETPW) strategy that incorporates a visible-light transparent broadband directional thermal emitter and a low-emissivity coating into commercial polycarbonate (PC) windows. In comparison to a PC window exposed to a 700 K thermal source at a half-view angle of 50°, the proposed NETPW exhibits remarkable temperature reduction (~77.7 ℃) by reflecting external radiation and enhancing directional radiative cooling. Simultaneously, the NETPW effectively inhibits heat emissions toward users, resulting in a significant improvement in thermal comfort, with a user's sensible temperature reduction of 57 ℃. Moreover, the NETPW exhibits high visible transparency, high-temperature resistance, scratch resistance, and impact resistance. The seamless integration with existing windows provides a novel approach for controlling thermal emission and optimizing energy exchange.

Keywords: Thermal protective window; Thermal comfort; Broadband directional thermal emission; Directional radiative cooling; Nanophotonics

Introduction

Thermal protection and comfort are crucial for safeguarding both instruments and individuals, particularly in high-temperature environments such as fires and steelworks[1-5]. Fire sources and furnaces often exceed 700 K. This substantial amount of thermal radiation poses a threat to the normal functioning of equipment and health risks to humans. Exposure to high-temperature thermal radiation can induce heat stress reactions in the human body, including heat stroke, dehydration, and heat exhaustion, which can lead to fatalities[6-7]. Effective thermal protection of the human body, particularly the face, is crucial when confronting high-temperature heat sources. Thermal protection windows are extremely important to ensure the safety of firefighters during fire rescue operations[8-12]. Therefore, such windows are essential for ensuring thermal protection and comfort for users[10-16].

Current thermal protective windows primarily employ transparent insulation materials featuring low thermal conductivity, such as polycarbonate (PC) and polymethyl methacrylate (PMMA)[17-22]. However, these materials exhibit high infrared absorption and radiation, thereby absorbing external radiation when exposed to high-temperature thermal sources and radiating heat to users; their temperatures can reach several hundred degrees. Consequently, they do not offer effective thermal protection and personal thermal comfort. In addition, their inadequate scratch resistance limits their commercial application in complex working environments. In the building sector, the use of low-emissivity (low-E) glasses involves the incorporation of a metal film to facilitate the efficient reflection of external thermal radiation[23-25]. However, their low infrared emissivity impedes their own thermal radiation, and their poor impact resistance presents challenges in applications such as fires and steelworks. In this context, the development of an advanced and efficient design method for thermal protective windows suited to complex high-temperature environments has been overlooked in current research.

In this paper, we present a dual-side nanophotonic-engineered thermal protective window (NETPW) strategy that incorporates a directional thermal emitter (DTE) and low-E coating into commercial PC windows. The DTE comprises epsilon-near-zero (ENZ), dielectric, and ENZ multilayer films (EDE) on the low-E coating. This coating, which faces users, is used to minimize thermal radiation toward the human body, whereas DTE-facing thermal sources are employed to reduce the external heat input and enhance passive directional radiative cooling. The fabricated NETPW provides users with better thermal protection and personal thermal comfort performance than a commercial PC window exposed to a high-temperature thermal source at different half-view angles (20–50°). Furthermore, the proposed NETPW exhibits excellent properties, including high visible transparency, high-

temperature resistance, scratch resistance, and impact resistance. This photonic-engineered dual-side thermal protection strategy, which facilitates integration with existing PC windows, offers new avenues for providing thermal protection and comfort to users through adaptation to complex high-temperature working environments.

Results

Principle and design

In this study, we considered a typical scenario of firefighting and steelworkers working in high-temperature environments (Fig. 1a). The system can be divided into three regions: high-temperature thermal source, thermal protective window, and users. High-temperature sources emit substantial heat in all directions. Thermal protection requires the temperature of protective windows to be as low as possible, whereas thermal comfort requires the sensible temperature of the user to be as low as possible. Therefore, the front side of thermal protective windows should reflect most of the thermal radiation from the thermal source to prevent the window from heating. However, the back side of the thermal protective windows facing the user should inhibit its thermal radiation to prevent the human body from heating. Combined with directional thermal emission, the thermal protective window should enhance the emission in specific directions outside the thermal source to achieve passive directional radiative cooling[26-28].

We designed an NETPW with broadband directional thermal emission by incorporating a DTE and low-E coating into commercial PC windows (Figs. 1b and 1c). The back side of the NETPW was a thin layer of transparent indium tin oxide (ITO) low-E coating. The low-E coating exhibits excellent electrical conductivity, resulting in low mid-infrared emissivity ($\varepsilon_{3\text{-}14\mu m}$~0.14) while still maintaining high visible transmittance ($T_{400\text{-}800nm}$>0.8). The front side of the NETPW is a DTE consisting of Al_2O_3, ZnS, and Al_2O_3 multilayer films on low-E coating. Note that Al_2O_3 is an ENZ material with longitudinal optical (LO) and transverse optical (TO) phonon polariton around 10.7 and 13 μm, respectively. The lossless dielectric ZnS is employed to realize a Fabry-Pérot (FP) cavity connecting the ENZ films. Directional thermal emission around 10.7 μm is enabled by the ultrathin Al_2O_3 layer on low-E coating through the Berreman mode[29-33]. Simultaneously, directional thermal emission around 13 μm is enabled by the Al_2O_3, ZnS, and Al_2O_3 multilayer films by combining FP resonances and the

Brewster effect[27]. By utilizing one ENZ material and a lossless dielectric film, the proposed DTE achieves broadband directional thermal emission covering the entire 8-14 μm atmosphere window.

To demonstrate passive directional radiative cooling performance, we used a system comprising a sample and a high-temperature thermal source (Fig. 1d). The sample radiates energy in emission directions spanning from θ_e to 90°. At θ_e=0°, the sample exhibits blackbody-like behavior, while at θ_e = 90°, it functions as a low-E film (Figs. 1e and S1) The half-view angle (α) of the sample is determined by the size of the external thermal source and the distance between the sample and the thermal source. The temperatures of the thermal source and surrounding environment were set to 700 K and 320 K, respectively. The resulting relationship between the calculated steady-state sample temperature and the directional emission angle (θ_e) for a given half-view angle (α=40°) is shown in Fig. 1e. When θ_e <40°, the sample temperature is lower than that of the blackbody, whereas when θ_e >40°, the sample temperature is lower than that of the ideal low-E film. The sample temperature is lowest when θ_e =α, indicating excellent passive directional radiative cooling performance. Therefore, the directional thermal emitter ($\theta_e \geqslant \alpha$) can achieve better radiative cooling performance than the blackbody or low-E coating when facing a high-temperature thermal source.

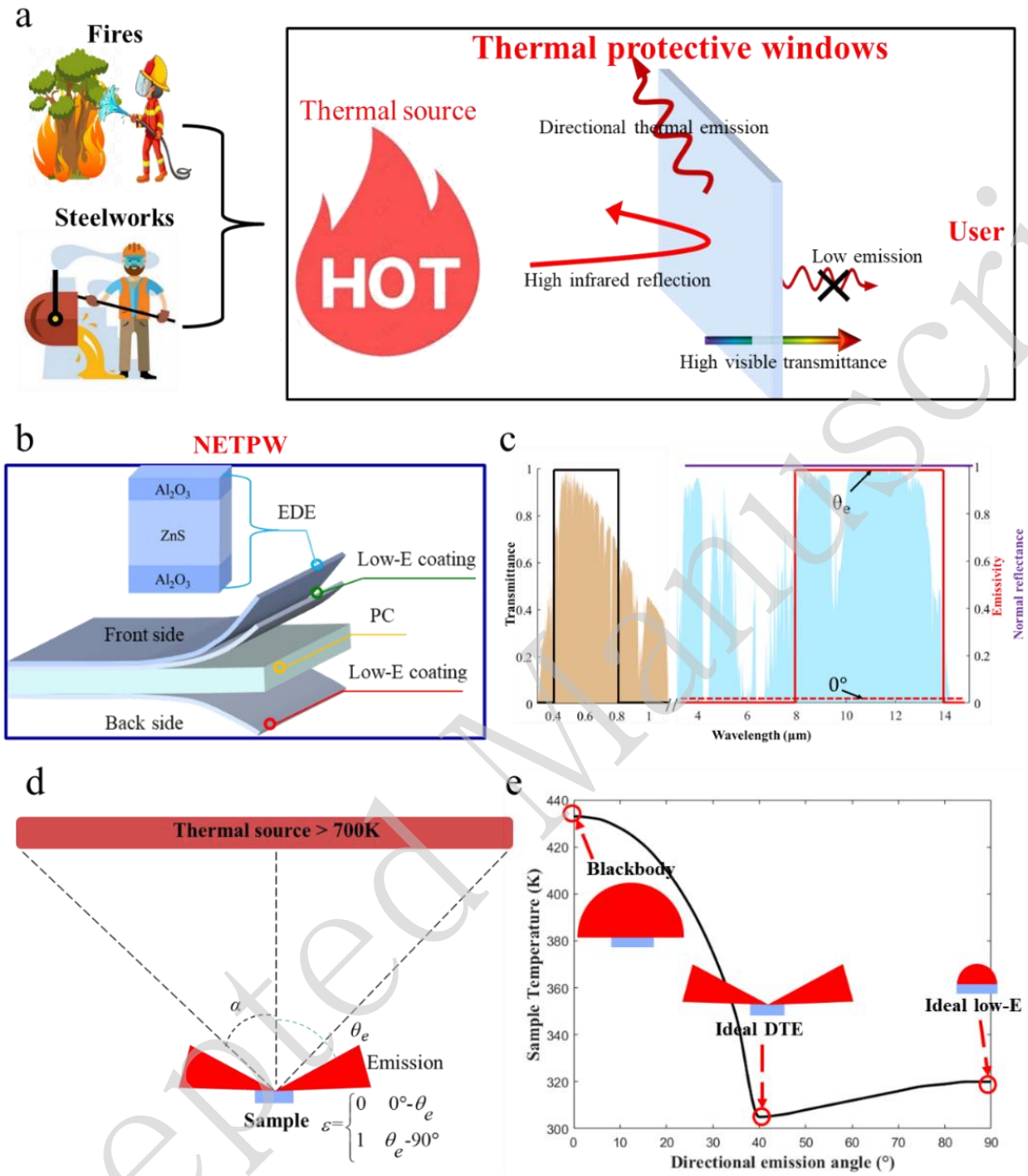

Fig. 1 Working principle of the NETPW. a Schematic of thermal protective windows used in typical high-temperature environments such as fires and steelworks. **b** Schematic structure of the thermal protective window. **c** Ideal spectra for the NETPW. The orange area denotes AM 1.5 solar spectrum. The light blue area denotes the atmosphere window. **d** Schematic of the directional thermal emitter when facing a high-temperature thermal source. **e** Relationship between the calculated steady-state sample temperature and the directional emission angle (θ_e) for a given half-view angle (α=40°) when the temperatures of the thermal source and surrounding environment were set to 700 K and 320 K, respectively.

Experimental and simulation results

An NETPW can be fabricated by covering the low-E coating on both sides of an existing commercial PC window. Subsequently, Al_2O_3, ZnS, and Al_2O_3 multilayer films must be deposited by E-beam evaporation (Fig. 2a). This film-based fabrication process is scalable for use in large windows, including those in buildings. Through simulation optimization, the thicknesses of the top Al_2O_3, ZnS, and bottom Al_2O_3 layers were determined to be 400, 1900, and 600 nm, respectively. The resulting NETPW exhibits high transmittance in the visible range ($T_{400\text{-}800nm}$>0.6) owing to the use of materials that possess visible transparency (Figs. 2a and S4). Moreover, the NETPW exhibits high mid-infrared normal reflection ($R_{3\text{-}14\mu m}$>0.8) due to the low-E coating, as shown in Fig. 2b. Therefore, the NETPW reflects most of the thermal radiation of the external thermal source to prevent the window from heating and provides thermal protection. Simultaneously, thermal radiation can be suppressed to prevent the human body from heating for personal thermal comfort.

To confirm the broadband directional thermal emission of the fabricated NETPW, we measured emissivity spectra at varying angles using a Fourier transform infrared spectrometer (Fig. S5). The experimental emissivity spectrum in p-polarization exhibits high emissivity (>0.5) at wide emission directions (50°-85°) covering the entire long-wave infrared atmospheric window (8-14 μm), which agrees well with the simulation results (Figs. 2c and 2d). To unveil the physics behind the broadband directional thermal emission, the normalized electric-field distribution and resistive loss in each layer were further investigated (Figs. 2e and 2f). The highly localized electric fields inside the ENZ and dielectric films constitute the physical origins of the Berreman and FP modes, respectively[29-33]. The high directional thermal emission around 10.7 μm is due to the Berreman mode, named LO absorption[32]. The high directional thermal emission around 13 μm is due to the synergistic effect of FP resonances and the Brewster effect, named TO absorption[28].

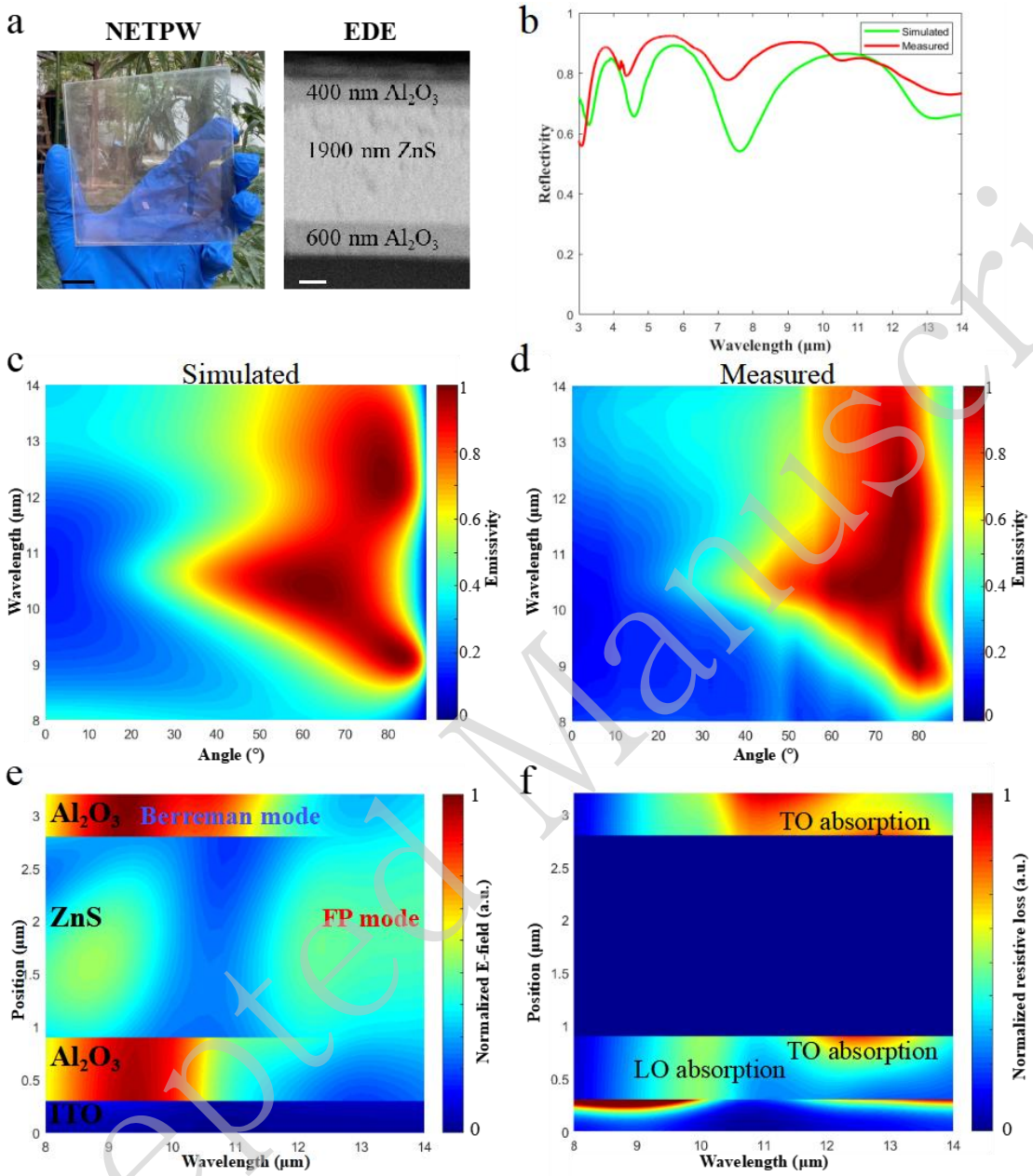

Fig. 2. Experimental and simulated results of the proposed NETPW. a Visible and scanning electron microscopy images of the fabricated NETPW. The black bar is 20 mm whereas the white bar is 500 nm. **b** Measured (red line) and simulated (green line) reflectivity spectra for the NETPW. **c** and **d** Measured and simulated emissivity spectra as functions of the angle for the fabricated NETPW in p-polarization. **e** and **f** Calculated normalized electric field distribution and resistive loss as functions of the wavelength for p-polarization at 70° angle of incidence. The normalized electric-field distribution and resistive loss are obtained by dividing the respective field strength and loss at each point by their maximum values within the region.

Thermal protection and thermal comfort performance

To demonstrate the thermal protection and thermal comfort performance of the proposed NETPW, we conducted a proof-of-concept experiment (Figs. 3a and S6). A ceramic hot table was used to simulate a 700 K external thermal source. The behavior of the human body, with a mid-infrared emissivity of approximately 0.98–0.99, can be approximated as that of a blackbody. Therefore, a thermally black object with an emissivity of 0.99 in the mid-infrared band was used to simulate a person's face in this proof-of-concept experiment[28]. The distance from the black object to the sample was 3 cm to simulate firefighters wearing protective face masks. The half-view angle (α) varies with the distance between the sample and the thermal source. The fabricated NETPW shown in Fig. 2a (i.e., sample E) was placed between the thermal source and artificial model, and the DTE side faced the thermal source. A commercial PC window (sample A), which behaved as a near-perfect blackbody, was used as a reference. The other reference samples were ITO-PC, PC-ITO, and ITO-PC-ITO, denoted as samples B, C, and D, respectively. T_1 and T_2 are the temperatures of the sample and artificial model, respectively.

Thermal protection requires the temperature of the sample to be as low as possible to prevent scalding of the human body. As shown in Fig. 3b, the NETPW (sample E) exhibited the lowest surface temperature among the five samples, indicating its excellent thermal protection performance. The temperature reduction between the NETPW (sample E) and PC window (sample A) increased with increasing half-view angle. When the half-view angle was 50°, the temperature reduction reached 77.7 ℃, indicating that the fabricated NETPW has better thermal protection performance than the commercial PC window. Because of the high infrared reflection of the low-E coating, most of the thermal radiation of the thermal source was reflected, thus preventing the window from heating. Therefore, the surface temperatures of the ITO-PC, ITO-PC-ITO, and DTE-PC-ITO samples were much lower than those of the PC and PC-ITO samples. Moreover, the surface temperatures of the DTE-PC-ITO sample were lower than those of the ITO-PC-ITO sample, indicating that the DTE has a good directional radiative cooling performance.

Thermal comfort requires the temperature of an artificial model to be as low as possible. As shown in Fig. 3c, the artificial model corresponding to the NETPW (sample E) exhibited the lowest surface temperature among the five samples, indicating the remarkable thermal comfort performance of the NETPW. The temperature reduction between the NETPW (sample E) and PC window (sample A) increases with the increasing half-view angle,

reaching 57 ℃ when the half-view angle was 50°. Therefore, the fabricated NETPW provides better thermal comfort performance than the commercial PC window. The proposed NETPW blocks direct thermal radiation from the thermal source to the human body; hence, the surface temperature of the artificial model is lower than that of the NETPW. Low-E coating on the back side passively inhibits its thermal radiation; hence, the surface temperatures of the artificial model corresponding to samples PC-ITO or ITO-PC-ITO are much lower than those of the artificial model corresponding to samples PC or ITO-PC. Moreover, the surface temperature of the artificial model corresponding to sample DTE-PC-ITO is lower than that of the artificial model corresponding to sample ITO-PC-ITO, indicating that the DTE has a good directional radiative cooling performance and reduces the thermal radiation output of the sample to the human body.

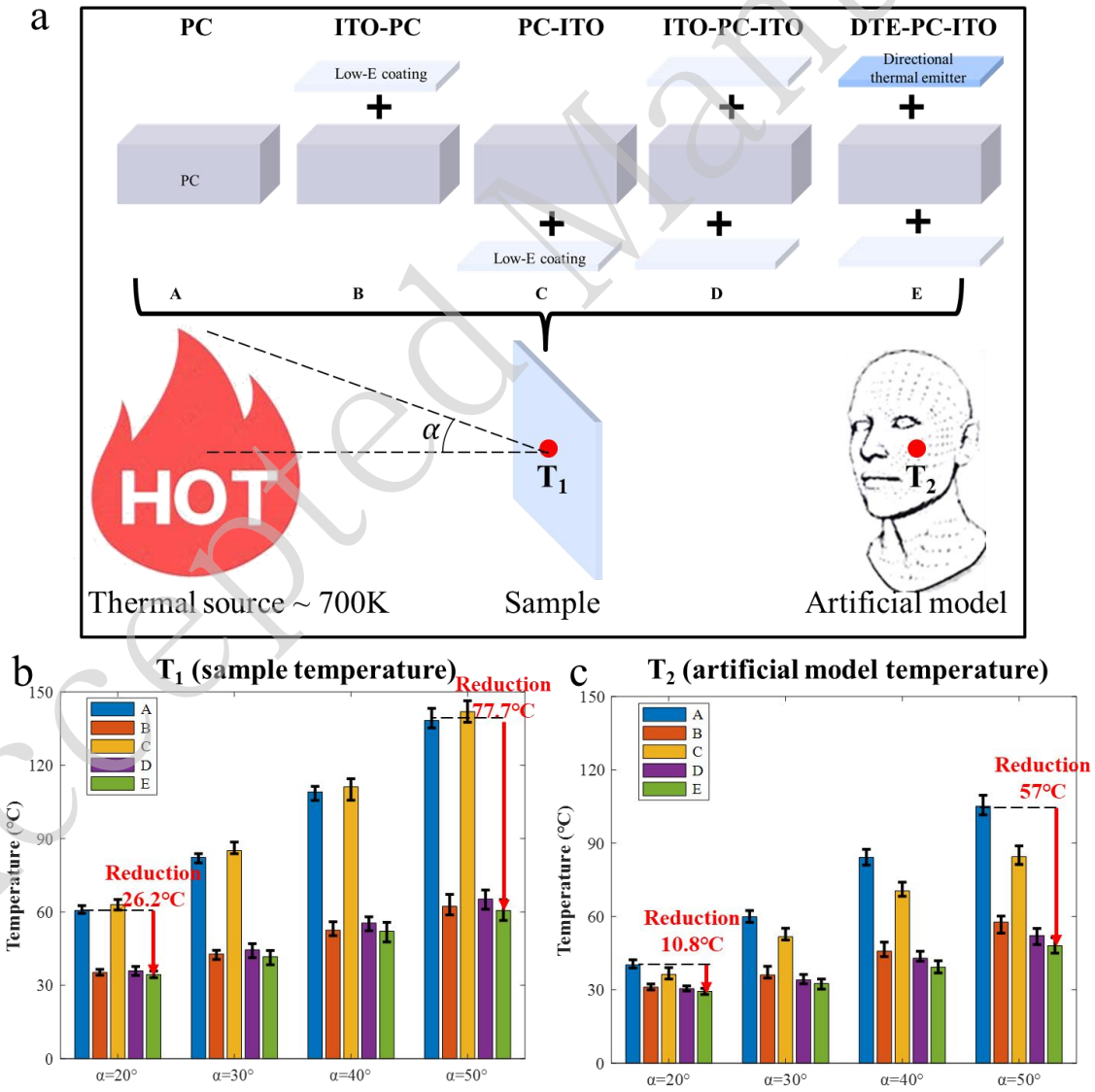

Fig. 3. Experimental demonstration of thermal protection and comfort performance of the thermal protective window. a Schematic of the experimental setup to demonstrate the thermal protection and comfort performance of the thermal protective window. The temperature of the thermal source was set to 700 K. The half-view angle (α) varies with the distance between the sample and the thermal source. **b** Surface temperatures of different samples at different half-view angles. The NETPW (sample E) achieves a temperature reduction compared to the PC window (sample A). **c** Surface temperatures of the artificial model at different half-view angles for different samples.

Thermal stability and mechanical properties

Compared to commercial PC windows, the proposed NETPW includes ITO, Al_2O_3, and ZnS materials, which have good visible transmittance, high-temperature resistance, and high hardness; hence, this NETPW maintains good thermal stability and mechanical properties. Direct radiometric measurements were performed using an IR camera to observe the thermal stability of the NETPW. Thus, the NETPW based on a commercial PC was placed on a 100 ℃ heating stage, exhibiting low radiation intensity similar to that of the Al sheet (ε~0.1) at 0° emission angle. By contrast, its radiation intensity notably increased and became comparable to that of the blackbody (ε~0.95) at 70° emission angle (Fig. 4a). This behavior indicates that the NETPW can efficiently radiate energy in target directions at a working temperature of 100 ℃. Furthermore, the high-temperature resistance of the NETPW can be improved by replacing the PC with a commercial high-temperature resistant polyimide (PI). Similarly, directional thermal radiation properties were observed at a working temperature of 250 ℃, as shown in Fig. 4a. Therefore, we conclude that the NETPW exhibits good high-temperature resistance and can be applied to high-temperature working environments such as fire disasters and steel smelting plants.

The mechanical durability of NETPWs is essential for protecting the eyes, face, and neck in real-world applications, where sparks, debris, and falling objects are common hazards in fires and steelworks. Mechanical performance is typically characterized by two aspects: scratch resistance and impact resistance. The hardness and elasticity modulus indicate the ability of the material to resist surface scratches or indentations, that is, whether the surface of the material is prone to scratches or deformation[34]. A high hardness and elasticity modulus indicate that the surface of the material is more difficult to scratch or deform. The hardness and elasticity modulus of the samples were measured using the nanoindentation technique (Figs. 4b and S7). The

nanoindentation hardness and elasticity modulus of the proposed NETPW (DTE-PC-ITO) exhibit a substantial increase, surpassing those of commercial PC windows by factors of 27.8 and 5.4, respectively. This notable enhancement can be attributed to the incorporation of the $Al_2O_3/ZnS/Al_2O_3$ multilayer film structure, which effectively enhances the scratch resistance. Moreover, this NETPW requires a higher impact energy to split, according to the falling-ball impact test (Figs. 4c and S8). Overall, the fabricated NETPW exhibits excellent scratch and impact-resistant mechanical properties, which are suitable for complex working environments.

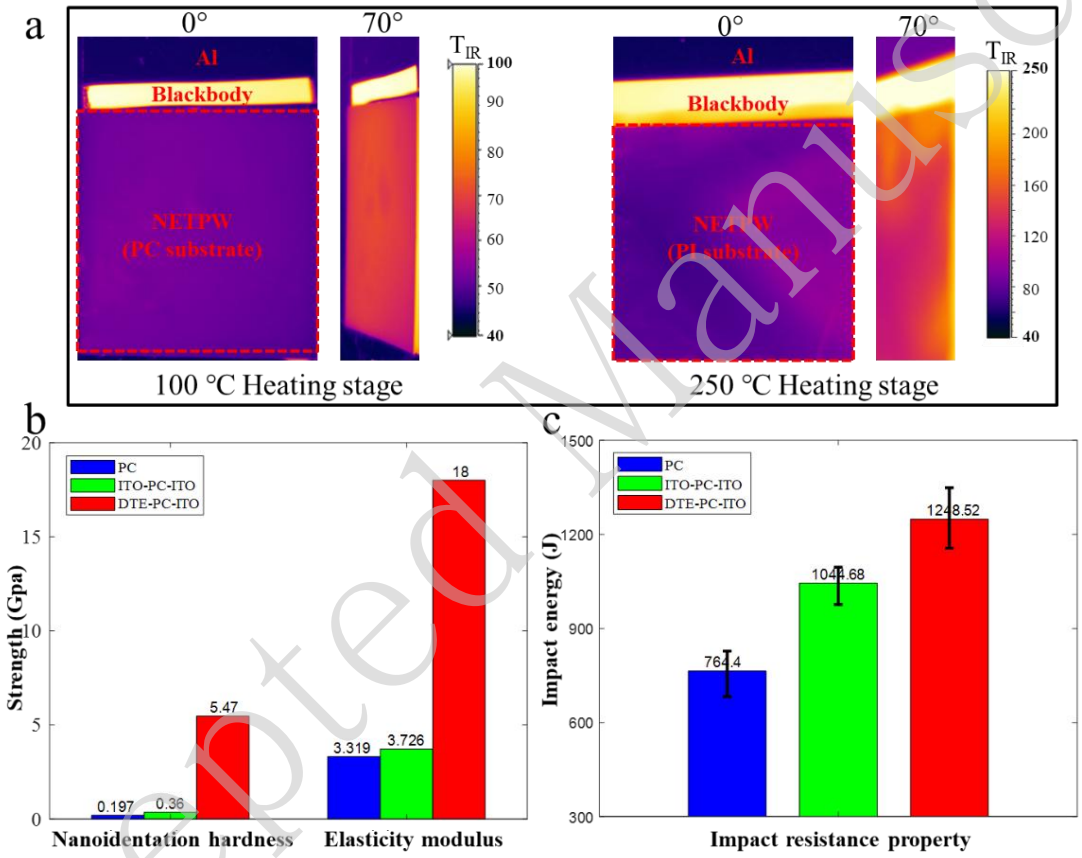

Fig. 4. Thermal stability and mechanical properties of the NETPW. a Thermal images of the fabricated NETPW based on PC substrate (left). The sample size was 100 × 100 mm^2 and was placed on a 100 ℃ heating stage. The Al sheet (ε~0.1) and blackbody (ε~0.95) were used as references placed next to the sample. Thermal images of the fabricated NETPW based on the flexible PI substrate (right). The sample size was 20 × 20 mm^2 and was placed on a 250 ℃ heating stage. **b** Nanoindentation hardness and elasticity modulus comparison of PC, ITO-PC-ITO, and DTE-PC-ITO samples. **c** Comparison of impact resistance property for PC, ITO-PC-ITO, and DTE-PC-ITO samples.

Discussion

We proposed and fabricated an NETPW with directional radiative cooling to provide users with thermal protection and personal thermal comfort in complex high-temperature working environments. First, the NETPW was implemented easily by coating the front and back sides of a commercial PC window with a visible-transparent broadband directional thermal emission film and a low-E film. This approach enables simultaneous control of the thermal emission spectrum and direction, allowing for customized radiative energy exchange in high-temperature environments. Additionally, the proposed broadband (8-14 μm) directional thermal emission surface facilitates energy-efficient directional radiative cooling, and its working wavelength ranges can be tailored by ENZ material choices. It is achieved using only one ENZ material, unlike previous broadband directional thermal emitters, which relied on the superposition of multiple ENZ materials. This further extends its applicability to various thermal management applications. Third, the easy fabrication procedure involving only film deposition makes this NETPW suitable for low-cost scalable manufacturing. Moreover, the fabricated NETPW has excellent optical, thermal, and mechanical properties, including high visible transparency, and high-temperature, scratch, and impact resistance, which is essential for special protection work, such as firefighting and steel-smelting[35, 36]. Ultimately, we believe that it has the potential for application in various fields, including space heating and cooling[37-47], and thermal management[48-56].

Materials and methods

Sample fabrication and preparation

The nanophotonic-engineered thermal protective window is composed of Al_2O_3/ZnS/Al_2O_3 multilayer films, top low-E coating, a middle spacer, and bottom low-E coating. The middle spacer is a commercial PC (100 × 100 × 2 mm^3) or PI (100 × 100 × 0.5 mm^3) with a high visible transmittance (>0.9). The low-E coating is a 200-μm-thick adhesive ITO-PET film featuring a square resistance of approximately 5 Ω. First, the low-E coating was pasted on both sides of the commercial PC window, and then a 600 nm Al_2O_3 film (deposition rate of 0.3 nm/s) was deposited with E-beam evaporation (Denton Vacuum, Explore 14) on one side, followed by a 1900 nm ZnS film (deposition rate of 0.4 nm/s) and 400 nm Al_2O_3 film (deposition rate of 0.3 nm/s).

Optical measurements

Visible transmission spectra (400-800 nm) were recorded using a universal measurement spectrophotometer (Agilent, Cary7000) equipped with an integrating sphere. The infrared reflectivity spectrum (3-14 μm) was acquired using a microscope (Hyperion 1000, Brucker) and a Fourier transform infrared spectrometer (Vertex 70, Brucker), in conjunction with an MCT detector. The infrared emissivity spectrum was measured using a Fourier-transform infrared spectrometer with MCT detectors, and carbon black deposited on a gold-coated silicon wafer was used as a blackbody reference. Thermal images in the long-wave infrared band were measured with an IR camera (Blackbird precision sl, Jenoptik) with a detection wavelength range of 8-14 μm.

Thermal measurements

As a proof of concept, a thermal protection and comfort experiment was conducted in which the fabricated sample (30 × 30 × 2.4 mm^3) was suspended between a hot table and a thermally black object (Fig. S6). A high-temperature ceramic hot table (Etool, ET-138200F) was used to simulate the 700 K external thermal source, and a thermally black object (30 × 30 × 2.4 mm^3) was used as an artificial model (i.e., a person's face). The distance from the black object to the sample was 3 cm to simulate near-distance applications, such as protective glasses and face masks. The distance from the black object to the sample could be adjusted using a lifting platform, and different distances corresponded to different half-view angles (α). Temperature measurements were performed using adhesive thermocouples (Omega, SA-1K) on the sample and artificial model, and a controller (KSB24A0R) was used to record the temperature in real time.

Mechanical measurements

Nanoindentation is a microscale technique that is used to test the surface mechanical properties of a material. During the test, an indenter was pressed into the surface of the material, and parameters such as load, indentation depth, and time were recorded. The load-displacement curve was drawn according to the parameters obtained by the nanoindenter (Agilent, G200) test. Finally, the mechanical properties of the material, such as the surface hardness and elastic modulus, were obtained (Figs. 4c and S7). The splitting impact energy of the sample was obtained using a falling-ball impact test (Figs. 4d and S8), and the sample size was 30 × 30 × 2.4 mm^3.

Numerical simulations

The simulated emissivity spectra, normalized electric field distribution, and normalized resistive loss were calculated using a radio frequency module (electromagnetic waves, frequency domain) in COMSOL Multiphysics.

Acknowledgements

This study was supported by the National Natural Science Foundation of China (Grant Numbers U2341225 and 62375242) and Sichuan Science and Technology Program (2025YFHZ0297). The authors thank Liying Chen from the State Key Laboratory of Extreme Photonics and Instrumentation, Zhejiang University, for her assistance with the FTIR experiments.

Conflict of interests

The authors declare no conflict of interests.

Contributions

Q.L. conceived the study and supervised the project. Y.Y. performed calculations and experiments. J.Y. participated in the thermal measurements. W.S. and P. G. performed part of the characterization. Y.Y. and P. G. prepared the manuscript. Q. L., M. Q., and P. G. reviewed and revised the manuscript. All the authors discussed the results and contributed to the final version of the manuscript.

References

1. Das, S. & Subudhi, S. A review on different methodologies to study thermal comfort. *International Journal of Environmental Science and Technology* **19**, 2155-2171 (2022).
2. Uyanna, O. & Najafi, H. Thermal protection systems for space vehicles: a review on technology development, current challenges and future prospects. *Acta Astronautica* **176**, 341-356 (2020).
3. Ilic, O. et al. Tailoring high-temperature radiation and the resurrection of the incandescent source. *Nature Nanotechnology* **11**, 320-324 (2016).
4. Carballo-Leyenda, B. et al. Wildland firefighters' thermal exposure in relation to suppression tasks. *International Journal of Wildland Fire* **30**, 475-483 (2021).
5. Su, Y. et al. Development of a numerical model to predict physiological strain of firefighter in fire hazard. *Scientific Reports* **8**, 3628 (2018).
6. Agostinelli, P. J. et al. Validity of heart rate derived core temperature estimation during simulated firefighting tasks. *Scientific Reports* **13**, 22503 (2023).
7. Acharya, J., Bhanja, D. & Dev Misra, R. Prediction of safe zone for firefighters exposed to purely radiant heat source-a numerical analysis. *International Journal of Thermal Sciences* **190**, 108302 (2023).
8. Wang, L. J. et al. Developing smart fabric systems with shape memory layer for improved thermal protection and thermal comfort. *Materials & Design* **221**, 110922 (2022).
9. Bartkowiak, G., Dąbrowska, A. & Greszta, A. Development of smart textile materials with shape memory alloys for application in protective clothing. *Materials* **13**, 689 (2020).
10. Peng, Y. C. et al. Coloured low-emissivity films for building envelopes for year-round energy savings. *Nature Sustainability* **5**, 339-347 (2022).
11. Nie, S. et al. Soft, stretchable thermal protective substrates for wearable electronics. *npj Flexible Electronics* **6**, 36 (2022).
12. Jung, Y. et al. Functional materials and innovative strategies for wearable thermal management applications. *Nano-Micro Letters* **15**, 160 (2023).
13. Yu, J. B. et al. Asymmetric directional control of thermal emission. *Advanced Materials* **35**, 2302478 (2023).

14. Liu, T. J. et al. Thermal photonics with broken symmetries. *eLight* **2**, 25 (2022).
15. Qin, B. et al. Whole-infrared-band camouflage with dual-band radiative heat dissipation. *Light*: *Science & Applications* **12**, 246 (2023).
16. Lin, K. T. et al. Highly efficient flexible structured metasurface by roll-to-roll printing for diurnal radiative cooling. *eLight* **3**, 22 (2023).
17. Sun, Y. Y., Wilson, R. & Wu, Y. P. A review of transparent insulation material (TIM) for building energy saving and daylight comfort. *Applied Energy* **226**, 713-729 (2018).
18. Ming, Y. et al. Optical evaluation of a smart transparent insulation material for window application. *Energy Conversion and Management*: *X* **16**, 100315 (2022).
19. Cao, C. F. et al. Fire intumescent, high-temperature resistant, mechanically flexible graphene oxide network for exceptional fire shielding and ultra-fast fire warning. *Nano-Micro Letters* **14**, 92 (2022).
20. Xue, T. T. et al. Fast and scalable production of crosslinked polyimide aerogel fibers for ultrathin thermoregulating clothes. *Nature Communications* **14**, 8378 (2023).
21. Leung, E. M. et al. A dynamic thermoregulatory material inspired by squid skin. *Nature Communications* **10**, 1947 (2019).
22. Gupta, N. & Tiwari, G. N. Review of passive heating/cooling systems of buildings. *Energy Science & Engineering* **4**, 305-333 (2016).
23. Frydrych, I. et al. Comparative analysis of the thermal insulation of traditional and newly designed protective clothing for foundry workers. *Polymers* **8**, 348 (2016).
24. Chou, C. et al. Physiological strains of wearing aluminized and non-aluminized firefighters' protective clothing during exercise in radiant heat. *Industrial Health* **49**, 185-194 (2011).
25. Liu, S. et al. Mask-inspired moisture-transmitting and durable thermochromic perovskite smart windows. *Nature Communications* **15**, 876 (2024).
26. Zhou, J. W. et al. Angle-selective thermal emitter for directional radiative cooling and heating. *Joule* **7**, 2830-2844 (2023).
27. Ying, Y. B. et al. Directional thermal emission covering two atmospheric windows. *Laser & Photonics Reviews* **17**, 2300407 (2023).

28. Cho, J. W. et al. Directional radiative cooling via exceptional epsilon-based microcavities. *ACS Nano* **17**, 10442-10451 (2023).
29. Xu, J., Mandal, J. & Raman, A. P. Broadband directional control of thermal emission. *Science* **372**, 393-397 (2021)
30. Liu, M. Q. et al. Broadband mid-infrared non-reciprocal absorption using magnetized gradient epsilon-near-zero thin films. *Nature Materials* **22**, 1196-1202 (2023).
31. Saha, S. et al. Tailoring the thickness-dependent optical properties of conducting nitrides and oxides for epsilon-near-zero-enhanced photonic applications. *Advanced Materials* **35**, 2109546 (2023).
32. Ying, Y. B. et al. Whole LWIR directional thermal emission based on ENZ thin films. *Laser & Photonics Reviews* **16**, 2200018 (2022).
33. Nordin, L. et al. Mid-infrared epsilon-near-zero modes in ultra-thin phononic films. *Applied Physics Letters* **111**, 091105 (2017).
34. Cheng, Y. T. & Cheng, C. M. Relationships between hardness, elastic modulus, and the work of indentation. *Applied Physics Letters* **73**, 614-616 (1998).
35. Maurya, A. K. et al. Effect of radiant heat exposure on structure and mechanical properties of thermal protective fabrics. *Polymer* **222**, 123634 (2021).
36. Zhou, J. Y. et al. Advanced functional Kevlar composite with excellent mechanical properties for thermal management and intelligent safeguarding. *Chemical Engineering Journal* **428**, 131878 (2022)
37. Ao, X. Z. et al. Self-adaptive integration of photothermal and radiative cooling for continuous energy harvesting from the sun and outer space. *Proceedings of the National Academy of Sciences of the United States of America* **19**, e2120557119 (2022).
38. Lee, M. et al. Photonic structures in radiative cooling. *Light*: *Science & Applications* **12**, 134 (2023).
39. Wu, X. K. et al. An all-weather radiative human body cooling textile. *Nature Sustainability* **6**, 1446-1454 (2023).
40. Zhu, Y. N. et al. Night-time radiative warming using the atmosphere. *Light*: *Science &*

Applications **12**, 268 (2023).

41. Li, D. et al. Scalable and hierarchically designed polymer film as a selective thermal emitter for high-performance all-day radiative cooling. *Nature Nanotechnology* **16**, 153-158 (2021).
42. Kang, M. H. et al. Outdoor-useable, wireless/battery-free patch-type tissue oximeter with radiative cooling. *Advanced Science* **8**, 2004885 (2021).
43. Xie, F. et al. Subambient daytime radiative cooling of vertical surfaces. *Science* **386**, 788-794 (2024).
44. Qin, B. et al. Space-to-ground infrared camouflage with radiative heat dissipation. *Light*: *Science & Applications*, **14**, 137 (2025).
45. Zhao, M. et al. High-temperature stealth across multi-infrared and microwave bands with efficient radiative thermal management. *Nano-Micro Letters* **17**, 199 (2025).
46. So, S. et al. Radiative cooling for energy sustainability: from fundamentals to fabrication methods toward commercialization. *Advanced Science* **11**, 2305067 (2024).
47. Liu, P. F. et al. Functional radiative cooling: basic concepts, materials, and best practices in measurements. *ACS Applied Electronic Materials* **5**, 5755-5776 (2023).
48. Khurgin, J. et al. Hot-electron dynamics in plasmonic nanostructures: fundamentals, applications and overlooked aspects. *eLight* **4**, 15 (2024).
49. Ergoktas, M. S. et al. Multispectral graphene-based electro-optical surfaces with reversible tunability from visible to microwave wavelengths. *Nature Photonics* **15**, 493-498 (2021).
50. Quan, C. et al. A Non-volatile switchable infrared stealth metafilm with GST. *Light: Advanced Manufacturing* **6**, 142-151 (2025).
51. Huang, Y. et al. Hierarchical visible-infrared-microwave scattering surfaces for multispectral camouflage. *Nanophotonics* **11**, 3613-3622 (2022).
52. Xu, Z. Q. et al. Spatially resolved dynamically reconfigurable multilevel control of thermal emission. *Laser & Photonics Reviews* **14**, 1900162 (2020).
53. Ma, Y. et al. Broadband unidirectional thermal emission. *Laser & Photonics Reviews* **19**, 2400716 (2024).
54. Heo, S. Y. et al. A *Janus* emitter for passive heat release from enclosures. *Science Advances* **6**,

eabb1906 (2020).

55. Xu, Z. Q. et al. Nonvolatile optically reconfigurable radiative metasurface with visible tunability for anticounterfeiting. *Nano Letters* **21**, 5269-5276 (2021).
56. Youngblood, N. et al. Reconfigurable low-emissivity optical coating using ultrathin phase change materials. *ACS Photonics* **9**, 90-100 (2022).